

Algorithm for Tracing Radio Rays in Solar Corona and Chromosphere

L. Benkevitch

MIT Haystack Observatory, Westford MA

and

I. Sokolov

AOSS, University of Michigan, Ann Arbor MI

and

D. Oberoi

MIT Haystack Observatory, Westford MA

and

T. Zurbuchen

AOSS, University of Michigan, Ann Arbor MI

ABSTRACT

In this paper a new efficient algorithm for computation of radio wave ray trajectories in isotropic media is described. The algorithm is based on an original second-order difference scheme with a specific “length-conservation” property, which allows to resolve the ray shape even in the regions where its curvature is high. Besides the scheme, the algorithm includes a number of mechanisms securing its correctness and stability. The algorithm is intended for obtaining multi-pixel solar images in wide range of radio frequencies, and it is designed to be used in studies of the solar environment with modern high-resolution radiointerferometers and radiotelescopes such as the Murchison Widefield Array (MWA).

1. Introduction

The problems of image simulation and reconstruction in solar radioastronomy require computation of multiple ray trajectories. A typical image of the sun consists of thousands to millions pixels, and the brightness of each of the pixels is obtained as an integral over an individual ray trajectory. Due to non-uniform distribution of the index of refraction in heliospheric plasmas at lower frequencies (up to a few GHz) the ray trajectories cannot be treated as straight lines. The ray-tracing problems require significant amount of computations, and, hence, time. It is possible to considerably reduce the computation time through the use of efficient ray-tracing algorithms.

In this work a ray tracing algorithm is presented. It allows one to calculate trajectories of electromagnetic rays in space plasmas with specified density distributions. In most applications the radio rays are traced to calculate certain physical quantities, such as intensity or black body brightness temperature, through path integration over the ray trajectories. In its software implementation the algorithm performs the integration and the ray trajectory calculation simultaneously.

We start with a brief review of the facts from the physics of electromagnetic wave propagation in plasmas pertinent to the ray tracing. We show the relationship between the plasma density, the dielectric permittivity, and the index of refraction

as well as between their gradients. In the next section we derive the ray equations from the Fermat's principle. We transform the set of ray equations so that their solution is a naturally parameterized curve. This representation reveals the mathematical analogy of the ray equations and the equations for a particle motion in magnetic field. Using this analogy, we derive a Crank & Nicolson (1947) second-order difference scheme using the Boris (1970) approach. In the Boris' scheme the particle energy, or the squared velocity, is conserved. For the naturally parameterized curve like that we use here the first derivative of the vector to be solved from the equation is not velocity (as present in the equation of the particle motion), but the unity-length direction cosine vector. Our scheme conserves the squared direction vector at unity. To achieve this, we employ the ideas which are often used while simulating the particle motion and which are known to conserve the velocity vector length in the magnetic field.

The difference scheme coding is quite straightforward, so in the section devoted to the numerical implementation of the algorithm we focus on discussing the ways to secure the algorithm robustness for the media with non-linear plasma density changing in space by presumably decades of orders of magnitude. This is shown to be the case for the heliosphere. We describe the methods we used to adaptively decrease and increase the integration step and the techniques used to avoid the ray penetration into the regions with the density above the critical. These methods are intended to reverse the ray direction and use parabolic and linear approximations of the trajectory.

In the testing and validation section we show the algorithm demonstrates excellent precision in the medium with one-dimensional linear plasma density gradient. In the example application section we verify the algorithm through solving a ray-tracing problem in the corona and chromosphere with realistic model density distributions, those by Saito (1970) and Cillie & Menzel (1935). Our algorithm implementation shows good results, demonstrated in a few plots of the ray beams refracting near the sun.

2. Fundamentals of ray refraction in isotropic plasmas

We treat the electromagnetic ray trajectory as a curve with radius vector \mathbf{r} in the three-dimensional space. For any starting point, \mathbf{r}_0 , and any given vector of initial direction, \mathbf{v}_0 , the whole shape of the ray trajectory may be unambiguously determined, as long as the distribution of the index of refraction, $n(\mathbf{r}, \omega)$, is known for a given angular frequency ω .

For the natural parameterization of the curve, $\mathbf{r}(s)$, where s is its arc length, the direction vector $\mathbf{v}(s)$ is defined as the first derivative of position vector, or $\mathbf{v}(s) = \mathbf{r}'(s)$. The components of $\mathbf{v}(s)$ are direction cosines, and $|\mathbf{v}(s)| = 1$ at any point of the curve. Here we show that the plasma density distribution, $\rho(\mathbf{r})$, suffices to determine the index of refraction $n(\mathbf{r})$ at a given wave frequency. In the Gaussian units, n is the square root of plasma dielectric permittivity, $n = \sqrt{\varepsilon}$. For isotropic plasmas

$$n^2 = 1 - \frac{\omega_p^2}{\omega^2}, \quad (1)$$

where the plasma frequency is $\omega_p = (4\pi e^2 n_e / m_e)^{1/2}$, e being the electron charge, m_e and n_e the electron mass and number density in the Gaussian (CGS) units. Under the quasineutrality condition the hydrogen plasma density is $\rho = m_p n_e$, where m_p is the proton mass, so the dielectric permittivity is expressed as

$$\varepsilon = 1 - \frac{\rho}{\rho_{cr}} \quad (2)$$

Here ρ_{cr} is the critical plasma density, at which the permittivity and, hence, the refraction index for the given frequency are zero:

$$\rho_{cr} = \frac{m_p m_e \omega^2}{4\pi e^2} \quad (3)$$

Electromagnetic rays of the frequency ω cannot travel in the regions with $\omega_p > \omega$, i.e. with $\rho > \rho_{cr}$ where the index of refraction takes imaginary values. The boundary between the region where $\rho < \rho_{cr}$ and the region with $\rho > \rho_{cr}$ is called the critical surface. The rays near the critical surfaces undergo strong refraction bending them away from the surface. In limit cases this effect is similar to the reflection.

The algorithm described further uses the relative gradient of refractive index, $\nabla n/n$. Since the permittivity gradient can be expressed from Eq. (2) as $\nabla \varepsilon = -\nabla \rho / \rho_{cr}$, the relative gradient of n is

$$\frac{\nabla n}{n} = \frac{\nabla \varepsilon}{2\varepsilon} = -\frac{\nabla \rho}{2(\rho_{cr} - \rho)} \quad (4)$$

Thus, if we know the critical density, the relative gradient of refractive index is totally determined by the plasma density and the density gradient.

3. Ray equation for isotropic media

To derive the equation for the ray trajectory we use the Fermat's principle. It states that a ray joining two points P_1 and P_2 will choose the path over which the integral of the refraction index, n , reaches its minimum, so that the variation of the integral about this path is zero:

$$\delta \int_{P_1}^{P_2} n(\mathbf{r}) ds \quad (5)$$

Notice that the integration in (5) occurs along a path, while in the Hamiltonian principle of least action the integration is with respect to the time. Transform the integrand of (5) into the form of the Lagrangian by changing s for a time-like independent variable τ . If $s = s(\tau)$, then $ds^2 = \dot{r}^2 d\tau^2$, where $\dot{r}^2 = \dot{\mathbf{r}} \cdot \dot{\mathbf{r}}$. Substitution of ds into (5),

$$\delta \int_{P_1}^{P_2} n(\mathbf{r}) \sqrt{\dot{r}^2} d\tau = 0, \quad (6)$$

turns the integrand into the Lagrangian $L(\mathbf{r}, \dot{\mathbf{r}}, \tau) = n(\mathbf{r}) \sqrt{\dot{r}^2}$. We apply the Euler method to (6) to find the vector differential equation of the curve satisfying the Fermat's principle. The Euler's equation is

$$\frac{d}{d\tau} \left(\frac{dL}{d\dot{\mathbf{r}}} \right) - \frac{dL}{d\mathbf{r}} = 0 \quad (7)$$

The Lagrangian derivatives with respect to $\dot{\mathbf{r}}$ and \mathbf{r} are

$$\frac{dL}{d\dot{\mathbf{r}}} = n(\mathbf{r}) \frac{\dot{\mathbf{r}}}{\sqrt{\dot{r}^2}} = n(\mathbf{r}) \frac{\dot{\mathbf{r}} d\tau}{\sqrt{\dot{r}^2} d\tau} = n(\mathbf{r}) \frac{d\mathbf{r}}{ds} \quad (8)$$

and

$$\frac{dL}{d\mathbf{r}} = \frac{dn(\mathbf{r})}{d\mathbf{r}} \sqrt{\dot{r}^2} = \nabla n(\mathbf{r}) \frac{ds}{d\tau}. \quad (9)$$

Therefore, the Euler's equation (7) for our problem (6) takes the form

$$\frac{d}{d\tau} \left(n \frac{d\mathbf{r}}{ds} \right) - \nabla n \frac{ds}{d\tau} = 0, \quad (10)$$

which, after multiplying both parts by $d\tau/ds$, yields the ray equation:

$$\frac{d}{ds} \left(n \frac{d\mathbf{r}}{ds} \right) - \nabla n = 0. \quad (11)$$

With the use of the vector identities, Eq. (11) can be represented in the format with explicit first and second derivatives of \mathbf{r} as

$$\frac{d^2 \mathbf{r}}{ds^2} = \frac{d\mathbf{r}}{ds} \times \left(\frac{\nabla n}{n} \times \frac{d\mathbf{r}}{ds} \right) \quad (12)$$

This is a system of three second-order equations. By introducing the direction vector $\mathbf{v} = d\mathbf{r}/ds$ the system (12) is transformed into the set of six first-order equations

$$\begin{cases} \frac{d\mathbf{r}}{ds} = \mathbf{v} \\ \frac{d\mathbf{v}}{ds} = \mathbf{v} \times \left(\frac{\nabla n}{n} \times \mathbf{v} \right) \end{cases} \quad (13)$$

The set of equations (13) is numerically solved by the proposed ray-tracing algorithm. Note that the independent variable s is the ray arc length so the solution to (13) is a naturally parameterized curve $\mathbf{r} = \mathbf{r}(s)$. This infers the "conservation law" for $\mathbf{v}(s) = \mathbf{r}'(s)$,

$$|\mathbf{v}| \equiv 1, \quad (14)$$

at any point of the curve. The algorithm of ray tracing described in Section 5 is based on a scheme that conserves this property.

4. Ray equation as particular case of Haselgrove equations

It is interesting to observe that equation (11) is a particular case of a more general set of ray equations derived by Walker (2008):

$$\begin{cases} \frac{d\mathbf{r}}{dt} = \nabla_k \omega(\mathbf{r}, \mathbf{k}) \\ \frac{d\mathbf{k}}{dt} = -\nabla \omega(\mathbf{r}, \mathbf{k}) \\ G(\omega, \mathbf{k}) = 0 \end{cases} \quad (15)$$

In Eqs. (15) $G(\omega, \mathbf{k}) = 0$ is the dispersion relation of the medium, t is time, $d\mathbf{r}/dt = \dot{\mathbf{r}} = \mathbf{V}_G$ is the group velocity of the wave packet, ω is the angular frequency, \mathbf{k} is the wave vector, and $\nabla_{\mathbf{k}}$ is the differentiation operator with respect to the \mathbf{k} components. System (15) is a modification of the Haselgrove (1955) equations. Its solutions are trajectories of rays of virtually any nature, not just electromagnetic, as long as the waves are plane and linear, varying in space and time as $\exp[i(\mathbf{k} \cdot \mathbf{r} - \omega t)]$.

Let us show that equation (11) is equivalent to system (15) for the waves traveling through a collisionless isotropic plasma with the dispersion relation

$$\omega^2 = c^2 k^2 - \omega_p^2, \quad (16)$$

which is easily found from equation (1) and the relation between the index of refraction and the magnitude k of the wave vector,

$$n = ck/\omega. \quad (17)$$

Hereafter c denotes the speed of light in the vacuum. In equations (15) we change variables, time t for arc length s . For a curve $\mathbf{r} = \mathbf{r}(t)$, where t is a parameter, the element of arc length

$$ds = |\dot{\mathbf{r}}| dt = |\mathbf{V}_G| dt. \quad (18)$$

Differentiation of (16) with respect to \mathbf{k} gives the first equation of system (15):

$$\frac{d\mathbf{r}}{dt} = \nabla_{\mathbf{k}} \omega = \frac{c^2}{\omega} \mathbf{k}, \quad (19)$$

and therefore the group velocity and its absolute value are

$$\mathbf{V}_G = \nabla_{\mathbf{k}} \omega = \frac{c^2}{\omega} \mathbf{k}, \quad V_G = \frac{c^2}{\omega} k. \quad (20)$$

Then, according to (18), dt is rendered as follows:

$$dt = \frac{\omega}{c^2 k} ds. \quad (21)$$

Substitution of dt in equation (19) yields

$$\frac{d\mathbf{r}}{ds} = \frac{\mathbf{k}}{k}. \quad (22)$$

The second equation of (15) is obtained in a similar way by applying ∇ to the dispersion relation (16),

$$\frac{d\mathbf{k}}{dt} = -\nabla \omega = -\frac{\omega_p}{c^2 k} \nabla \omega_p, \quad (23)$$

and using (21) to change dt for ds :

$$\frac{d\mathbf{k}}{ds} = -\frac{\omega_p}{c^2 k} \nabla \omega_p. \quad (24)$$

We reduce equation (22) to a form similar to that of (11). Multiply both sides by ck/ω and use (17):

$$n \frac{d\mathbf{r}}{ds} = \frac{c}{\omega} \mathbf{k}. \quad (25)$$

Differentiate both sides with respect to ds :

$$\frac{d}{ds} \left(n \frac{d\mathbf{r}}{ds} \right) = \frac{c}{\omega} \frac{d\mathbf{k}}{ds}. \quad (26)$$

Substitution of (24) in the right-hand-side yields

$$\frac{d}{ds} \left(n \frac{d\mathbf{r}}{ds} \right) = -\frac{\omega_p}{\omega ck} \nabla \omega_p. \quad (27)$$

The left-hand-side of (27) is the same as the first term in (11), while its right-hand-side is ∇n . This can be verified by applying ∇ operator to equation (1) and using the dispersion relation (16). Thus we have shown that equation (11) derived directly from the Fermat's principle in the previous Section is equivalent to the general ray equations (15) constrained by the conditions of plasma isotropy and absence of losses.

5. Algorithm description

The integration of system (13) is based on an original algorithm developed as a modification of the Boris' implementation of the explicit Crank & Nicolson (1947) scheme for the calculation of a charged particle motion in magnetic field (Hockney & Eastwood 1988). The Boris (1970) CYLRAD algorithm secures the energy conservation, which is equivalent to conservation of the particle's squared velocity \mathbf{v}^2 . The ray trajectory calculations require a different (though similar) conservation law to be observed.

Below is shown a brief derivation of the second-order difference scheme for the system (13). We introduce a vector quantity $\boldsymbol{\Omega}$ as

$$\boldsymbol{\Omega} = \frac{\nabla n}{n} \times \mathbf{v} \quad (28)$$

Substitute (28) into (13) to render the ray equations in the form

$$\begin{cases} \frac{d\mathbf{r}}{ds} = \mathbf{v} \\ \frac{d\mathbf{v}}{ds} = \mathbf{v} \times \boldsymbol{\Omega}. \end{cases} \quad (29)$$

Formally, this set of equations is the same as (4-90) in the book by Hockney & Eastwood (1988). However, in the ray trajectory equations (29) the independent variable s , the ray arc length, replaces the time t , introducing the natural ray parameterization. The ray direction $\mathbf{v}(s) = \mathbf{r}'(s)$ is used instead of the particle velocity $\mathbf{v}(t) = \mathbf{r}'(t)$, and the vector $\mathbf{\Omega}(s)$ is used instead of the cyclotron frequency $\mathbf{\Omega} = q\mathbf{B}/m$. Analogously, the square of direction vector $\mathbf{v}^2(s) = 1$ must also be conserved in the course of numerical integration, because $\mathbf{v}^2(s) = \mathbf{r}'^2(s) \equiv 1$ for any regular point of a naturally parameterized curve.

It is easy to show that $\mathbf{\Omega}$ is a vector whose length equals the ray curvature, defined as $\kappa = |\mathbf{r}''(s)|$ for naturally parameterized curves. Render the second equation in (29) as $\mathbf{r}'' = \mathbf{r}' \times \mathbf{\Omega}$. Multiply both sides of it by $\mathbf{r}' \times$ on the left:

$$\mathbf{r}' \times \mathbf{r}'' = \mathbf{r}' \times (\mathbf{r}' \times \mathbf{\Omega}) \quad (30)$$

Expanding the right-hand-side with the use of the vector identity and keeping in mind that $\mathbf{r}' \cdot \mathbf{r}' = 1$ and $\mathbf{r}' \perp \mathbf{\Omega}$, we get

$$\mathbf{\Omega} = -\mathbf{r}' \times \mathbf{r}'' \quad (31)$$

But for the natural parameterization $\mathbf{r}' \perp \mathbf{r}''$, hence, $|\mathbf{\Omega}| = |\mathbf{r}''|$, and

$$|\mathbf{\Omega}| = \kappa \quad (32)$$

The numerical solution is sought at the nodes of one-dimensional grid marked on the ray trajectory. Consider a grid whose nodes with respect to some i -th position are numbered as ... $(i-1)$, $(i-1/2)$, (i) , $(i+1/2)$, $(i+1)$,... and so forth. We subscript a variable with 0 if its value is taken at i -th point, with $(1/2)$ for $(i+1/2)$ -th point, and with 1 for $(i+1)$ -th point. A leapfrog difference scheme is used, where the half-step points are used in calculations. Suppose a ray at a particular moment has its end position \mathbf{r}_0 and direction \mathbf{v}_0 . The ray tracing scheme provides formulae to calculate its successive position \mathbf{r}_1 and direction \mathbf{v}_1 after the step ds along the ray arc length. The variables subscripted with $1/2$ are intermediate and they are related to the middle of the step. Note that the density and its gradient are provided only once for each step at the step middle point so the $(\nabla n/n)$ ratio is ascribed to the grid point $(i+1/2)$.

The second differential equation in (29) can be approximated by the differences as

$$\frac{\mathbf{v}_1 - \mathbf{v}_0}{ds} = \mathbf{v}_{1/2} \times \mathbf{\Omega}_{1/2} \quad (33)$$

Approximation of $\mathbf{v}_{1/2}$ as $\frac{1}{2}(\mathbf{v}_1 + \mathbf{v}_0)$ yields the implicit Crank & Nicolson (1947) scheme

$$\mathbf{v}_1 - \mathbf{v}_0 = (\mathbf{v}_1 + \mathbf{v}_0) \times \mathbf{\Omega}_{1/2} \frac{ds}{2} \quad (34)$$

This scheme has the benefit of unconditional stability. Multiply both sides of (34) scalarly by $\mathbf{\Omega}_{1/2}$ to get the property:

$$\mathbf{v}_1 \cdot \mathbf{\Omega}_{1/2} = \mathbf{v}_0 \cdot \mathbf{\Omega}_{1/2}, \quad (35)$$

which will be used later. To convert scheme (34) into the explicit one, express \mathbf{v}_1 from (34) as

$$\mathbf{v}_1 = \mathbf{v}_0 + (\mathbf{v}_1 + \mathbf{v}_0) \times \mathbf{\Omega}_{1/2} \frac{ds}{2} \quad (36)$$

and substitute it in the right-hand-side of (34) for itself. It yields

$$\begin{aligned} \mathbf{v}_1 = \mathbf{v}_0 + 2\mathbf{v}_0 \cdot \mathbf{\Omega}_{1/2} \frac{ds}{2} \\ + \left((\mathbf{v}_1 + \mathbf{v}_0) \times \mathbf{\Omega}_{1/2} \frac{ds}{2} \right) \times \mathbf{\Omega}_{1/2} \frac{ds}{2} \end{aligned} \quad (37)$$

Using the identity $\mathbf{v}_0 = \mathbf{v}_0(1 + (\mathbf{\Omega}_{1/2} \frac{ds}{2})^2 - (\mathbf{\Omega}_{1/2} \frac{ds}{2})^2)$, vector identities, property (35), and rearranging the terms, we arrive at the explicit difference scheme known as the Boris' CYLRAD algorithm (Boris 1970):

$$\begin{aligned} \mathbf{v}_1 = \mathbf{v}_0 + \frac{2}{1 + (\mathbf{\Omega}_{1/2} \frac{ds}{2})^2} \\ \left(\mathbf{v}_0 + \mathbf{v}_0 \times \mathbf{\Omega}_{1/2} \frac{ds}{2} \right) \times \mathbf{\Omega}_{1/2} \frac{ds}{2} \end{aligned} \quad (38)$$

The vector $\mathbf{\Omega}_{1/2}$ requires extrapolation: as seen from (28), the first multiplier, $\nabla n/n$, is obtained at the intermediate point and therefore has the $(1/2)$ subscript, while the second, \mathbf{v} , is only available for the starting point subscripted with 0. We denote this cross-product as $\mathbf{\Omega}_0$,

$$\mathbf{\Omega}_0 = \left(\frac{\nabla n}{n} \right)_{\frac{1}{2}} \times \mathbf{v}_0, \quad (39)$$

and use it as an initial value for $\mathbf{\Omega}$ extrapolation up to $\mathbf{\Omega}_{1/2}$. The half-step difference scheme for the second equation in (29) is

$$\mathbf{v}_{1/2} = \mathbf{v}_0 + \mathbf{v}_0 \times \mathbf{\Omega}_0 \frac{ds}{2} \quad (40)$$

Substitution of $\mathbf{v}_{1/2}$ into (28) yields the extrapolated $\mathbf{\Omega}$:

$$\mathbf{\Omega}_{1/2} = \left(\frac{\nabla n}{n} \right)_{\frac{1}{2}} \times \left(\mathbf{v}_0 + \mathbf{v}_0 \times \mathbf{\Omega}_0 \frac{ds}{2} \right) \quad (41)$$

In order to make the algorithm faster we reduce the number of multiplications. Note that all the occurrences of $\mathbf{\Omega}$ in (38) and (41) have the multiplier $ds/2$, so it is expedient to include it in the expressions for $\mathbf{\Omega}$ in (39) and (41). Finally, we put together the formulae (39), (41), and (38) and add the position vector \mathbf{r} adjustments at the start and the end to form the ray tracing algorithm (42).

The algorithm presented below converts the initial ray position and direction ($\mathbf{r}_0, \mathbf{v}_0$) into the new ones ($\mathbf{r}_1, \mathbf{v}_1$) along the ray path in five steps:

$$1. \mathbf{r}_{1/2} = \mathbf{r}_0 + \mathbf{v}_0 \frac{ds}{2} \quad (42a)$$

$$2. \mathbf{\Omega}_0 = \left(\frac{\nabla n}{n} \right)_{\frac{1}{2}} \times \mathbf{v}_0 \frac{ds}{2} \quad (42b)$$

$$3. \mathbf{\Omega}_{1/2} = \left(\frac{\nabla n}{n} \right)_{\frac{1}{2}} \times (\mathbf{v}_0 + \mathbf{v}_0 \times \mathbf{\Omega}_0) \frac{ds}{2} \quad (42c)$$

$$4. \mathbf{v}_1 = \mathbf{v}_0 + \frac{2}{1 + (\mathbf{\Omega}_{1/2} \frac{ds}{2})^2} (\mathbf{v}_0 + \mathbf{v}_0 \times \mathbf{\Omega}_{1/2}) \times \mathbf{\Omega}_{1/2} \quad (42d)$$

$$5. \mathbf{r}_1 = \mathbf{r}_{1/2} + \mathbf{v}_1 \frac{ds}{2} \quad (42e)$$

The first step (42a) provides the \mathbf{r} half-step-ahead approximation $\mathbf{r}_{1/2}$. Next two steps (42b) and (42c) calculate the half-step-ahead approximation for $\mathbf{\Omega}$. The fourth step (42d) estimates the new ray direction, \mathbf{v}_1 , based on the previous direction, \mathbf{v}_0 , and $\mathbf{\Omega}_{1/2}$. Step five, (42e), produces the new ray position, \mathbf{r}_1 , through the half-step from the intermediate point $\mathbf{r}_{1/2}$ along the new direction \mathbf{v}_1 .

6. Numerical implementation

The optical properties of the media where tracing the electromagnetic rays is of interest are often extremely nonuniform. For example, the electron number density N_e within the chromosphere alone falls off with the height by more than 10 orders of magnitude. Inside the solar corona N_e decays with the solar distance also by decades of magnitude orders. The index of refraction, as the square root of proportional to N_e dielectric permittivity (2), can change by many orders of magnitude within the region of study. The non-linear dependence of the refractive index on the wavelength poses other issues. For different wavelengths the ray geometry can be very different because the regions with the density greater than critical (3) form different configurations in space. The numerical implementation of algorithm therefore must include the mechanisms for adaptive step size ds adjustment not only to ensure the specified precision but also to prevent the ray from penetration into the region with $\rho > \rho_{cr}$. In some cases \mathbf{r}_0 appears so close to the region with the critical density that the step ds must be shorter than the absolute minimum step specified. For this condition a special method of replacing the ray trajectory by a segment of parabola or even straight line is used. All these techniques are described in this Section.

In our implementation of the ray tracing algorithm, aimed at obtaining multi-pixel images, many rays are processed simultaneously. Over a single integration step each of the rays is tested for precision and correctness, and only those that passed the tests are submitted to the Boris's algorithm to calculate new positions and directions. The rays for which the absolute minimum step leads to penetration to the region with $\rho > \rho_{cr}$ are switched to the opposite parabola branches or just reflected from the critical surface. The rest are the rays whose step sizes are too large to secure the specified precision. The step size for them is shortened by applying formula (46). The rays with reduced step sizes are processed at the next integration step. If a ray is leaving the dense region, its step size ds is increased over the series of subsequent integration steps.

The plasma density, ρ , and its gradient, $\nabla \rho$, are calculated through calls to the specialized subroutine once per each algorithm step. It is as-

sumed that these plasma parameters are obtained through an MHD simulation and they are available at the nodes of a three-dimensional grid with variable grid step. The same subroutine provides the estimate for the maximum ray step size consistent with the MHD grid size for each ray.

6.1. Precision control through adaptive step size

The desired precision of the ray trajectory is specified with the variable Tol . It has the meaning of inverse number of the steps n_s per a radian of the ray arc length. For example, $Tol < 0.1$ means that at least 10 steps per one radian of ray arc length is required. At each algorithmic step the real precision is calculated and compared with Tol , and if it exceeds Tol , the step ds is decreased.

The curvature κ is defined as the inverse of instant curvature radius as $\kappa = 1/R_c$. The actual ray curvature is available at each algorithm step as $|\mathbf{\Omega}|$ due to (32). Instead of the real precision it is convenient to use the quantity τ^2 , which is actually a halved real precision:

$$\tau^2 = \left(\mathbf{\Omega} \frac{ds}{2} \right)^2 = \left(\kappa \frac{ds}{2} \right)^2, \quad (43)$$

The algorithm step (42d) requires calculation of τ^2 anyway, so using it saves time. It is τ^2 that is compared with Tol^2 to make decision on the ds reduction. Comparing the halved real precision with the desired precision Tol makes the step adjustment less frequent as the specified precision is secured over most of the ray trajectory portions. To reduce the number of floating-point calculations, the τ^2 approximation uses the condition $\mathbf{v}^2 = 1$ in the identity $(\mathbf{u} \times \mathbf{v})^2 = \mathbf{u}^2 \mathbf{v}^2 - (\mathbf{u} \cdot \mathbf{v})^2 = \mathbf{u}^2 - (\mathbf{u} \cdot \mathbf{v})^2$. The index of refraction n in (28) is replaced by the dielectric permittivity as defined in (4), so

$$\tau^2 = \left(\frac{ds}{2} \left(\frac{\nabla \varepsilon_{1/2}}{2\varepsilon_{1/2}} \right) \times \mathbf{v}_0 \right)^2, \quad (44)$$

which with the use of the identity yields

$$\tau^2 = \left(\frac{ds}{2} \right)^2 \left[\left(\frac{\nabla \varepsilon_{1/2}}{2\varepsilon_{1/2}} \right)^2 - \left(\frac{\nabla \varepsilon_{1/2}}{2\varepsilon_{1/2}} \cdot \mathbf{v}_0 \right)^2 \right] \quad (45)$$

The step must be $ds = R_c/n_s = Tol/\kappa$ to have exactly $1/Tol$ points per radian of the ray, so due

to (43) it is corrected as:

$$ds' = \frac{Tol}{\sqrt{\tau^2}} \frac{ds}{2}, \quad (46)$$

The subroutine that provides the plasma density and density gradient at each call also provides the desired new step size ds_{new} for each ray. After the positions and directions for the rays have been advanced with the current step sizes, the algorithm attempts to increase the steps towards ds_{new} . However, ds_{new} can be greater than the current ds by orders of magnitude, and near the critical surface a simple assignment $ds = ds_{new}$ would almost inevitably lead to the ray penetration past the critical surface. Therefore the algorithm uses a special method for gradual increase of the step size. It is based on running a non-linear difference scheme which outputs the increased ds' from the current ds and the desired ds_{new} .

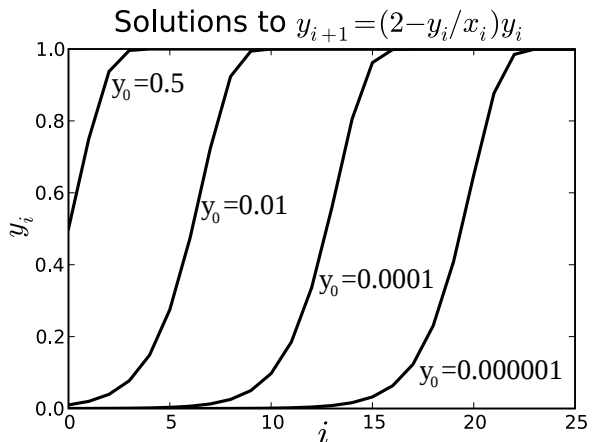


Fig. 1.— Solutions to the non-linear difference equation (47) for four different initial conditions y_0 . The input variable is constant: $x_i = 1$. The solutions, y_i , are increasing functions, always converging to $x_i = 1$. This scheme is used to smoothly increase the step ds to the set value of ds_{new} .

Consider a difference equation associating two variables, the input x and the output y , specified at the points ... (i-1), (i), (i+1), (i+2) ... and so on:

$$y_{i+1} = \left(2 - \frac{y_i}{x_i} \right) y_i \quad (47)$$

For constant input $x_i = X$ the solution to Eq. (47) is stable for any initial condition on the output variable y_0 between 0 and X . The solution to

Eq. (47) always converges to the value X . The useful property of Eq. (47) is that for a small (compared to X) initial condition y_0 the solution behaves similar to growing exponential function e^t , while for large values of y_0 , i.e. those closer to the X , it grows slower and slower similar to the decaying exponent Xe^{-t} , eventually converging to X . This behavior is illustrated in Fig. 1. Notice that reasonably large initial values for y_0 ensure fast convergence within 1% of the range $[0..1]$: 10 steps for $y_0 = 0.01X$, and even 3 steps for $y_0 = 0.5X$.

In our algorithm implementation the step ds is incremented using the Eq. (47) as the algorithm

$$ds' = \left(2 - \frac{ds}{ds_{new}}\right) ds \quad (48)$$

When ds is small compared to ds_{new} , each next value of ds' is almost $2ds$, so ds grows in a geometrical progression. However, as ds approaches ds_{new} , its growth rate becomes slower. These features ensure fast and yet smooth adjustment of ds in several steps up to the specified ds_{new} value.

6.2. Correctness control

Correctness of the ray path computation is violated if at some step the ray penetrates the critical surface. This condition can arise for very steep rays, almost normally incident on the critical surface. To prevent a ray from trespassing the critical surface the algorithm makes a linear prediction on the next value of dielectric permittivity ε . If the predicted ε is negative, the ray is approximated by a parabola and it is then switched to the symmetrical point on the opposite branch of the parabola. This is similar to the reflection at the critical surface, after which the ray starts traveling away from it. However, the linear ε prediction may fail due to highly non-linear plasma density distribution and then the ray trespasses the critical surface. This unphysical condition is corrected by returning the ray its previous position and direction, numerical calculation of the distance to critical surface along this direction, and linear reflection of the ray at the critical surface.

When the current ray state is $(\mathbf{r}_0, \mathbf{v}_0)$ and the algorithm is calculating its next position and direction $(\mathbf{r}_1, \mathbf{v}_1)$, the mid-step values of the plasma

density $\rho_{1/2}$ and its gradient $\nabla\rho_{1/2}$ are obtained from the subroutine, so the dielectric permittivity $\varepsilon_{1/2} > 0$ and its gradient $\nabla\varepsilon_{1/2}$ are available from (2) and (4), respectively. If the ray at next step occasionally trespasses the critical surface, the next value of permittivity, $\varepsilon_{3/2}$, will be negative. Therefore, predicting the sign of $\varepsilon_{3/2}$ helps the algorithm to make decision whether to use the Boris' scheme (42) or take measures to avoid the penetration past the critical surface. The prediction is based on testing the condition

$$\varepsilon_{3/2}/\varepsilon_{1/2} > 0 \quad (49)$$

Replace both numerator and denominator in (49) by the linear portions of their Taylor series:

$$\begin{aligned} \frac{\varepsilon_{3/2}}{\varepsilon_{1/2}} &= \frac{\varepsilon_0 + \mathbf{v}_0 \cdot \nabla\varepsilon_{1/2} 3 \frac{ds}{2}}{\varepsilon_0 + \mathbf{v}_0 \cdot \nabla\varepsilon_{1/2} \frac{ds}{2}} \\ &= 1 + \frac{\mathbf{v}_0 \cdot \nabla\varepsilon_{1/2}}{\varepsilon_0 + \mathbf{v}_0 \cdot \nabla\varepsilon_{1/2} \frac{ds}{2}} ds > 0, \end{aligned} \quad (50)$$

where ε_0 is the permittivity value at the point \mathbf{r}_0 . After rearranging the terms and dividing both parts by ε_0 we arrive at the correctness criterion:

$$\frac{ds}{2} \left(\mathbf{v}_0 \cdot \frac{\nabla\varepsilon_{1/2}}{\varepsilon_0} \right) > -\frac{1}{3} \quad (51)$$

Since the plasma density subroutine provides only the half-step value, $\rho_{1/2}$ and, hence, only the half-step permittivity value, $\varepsilon_{1/2}$, can be directly calculated, ε_0 is obtained as its back approximation using the linear terms of its Taylor series:

$$\varepsilon_0 = \varepsilon_{1/2} - \mathbf{v}_0 \cdot \nabla\varepsilon_{1/2} \frac{ds}{2} \quad (52)$$

If inequality (51) is true, the next step is supposed to be safe. If not, the ray is so close to the critical surface and so steep that it will penetrate the critical surface at the current step ds . In this case the next position and direction are calculated through parabolic approximation.

6.2.1. Parabola switching

This method is used when the correctness criterion (51) fails and the ray is about to trespass the critical surface. If the step ds is small enough, the dielectric permittivity gradient $\nabla\varepsilon$ can be considered constant over the ray path. In the medium

with $\nabla\varepsilon = \text{const}$ the electromagnetic rays have parabolic trajectories, which will be shown further. Knowing the parameters of the parabola (see Fig. 2), the algorithm calculates the position and direction vectors ($\mathbf{r}_1, \mathbf{v}_1$) of the ray at the symmetric point of the opposite branch of the parabola. The ray is switched to the opposite parabolic trajectory branch so that instead of approaching the critical surface it starts departing it. In order to find the new position and direction after the parabola switching we solve the ray Eq. (11) in two dimensions in the XY -plane containing the vectors $-\nabla\varepsilon_0$ and \mathbf{v}_0 , the X axis collinear with $-\nabla\varepsilon_0$.

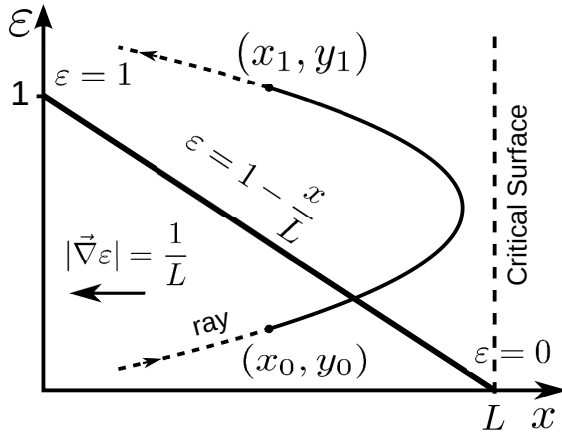


Fig. 2.— In a medium with linearly changing dielectric permittivity ε electromagnetic ray trajectories are second-order parabolae. The ε linearly changes from 1 at $x = 0$ to 0 at $x = L$. The critical surface is the locus where $\varepsilon = 0$.

Consider a simple 2-dimensional case of a ray traveling within the XY -plane, where the dielectric permittivity changes linearly from $\varepsilon = 1$ at the origin of coordinates down to $\varepsilon = 0$ at some distance L along the X axis, so that

$$\varepsilon = 1 - \frac{x}{L} \quad (53)$$

The case schematic is shown in Fig. 2. We shall derive the equation for the ray trajectory passing through an arbitrary point (x_0, y_0) . The equation set for the ray trajectory (11) in the two-dimensional geometry consists of two equations for x and y . The dielectric permittivity ε changes in the X direction only, so does the index of refraction n , therefore its gradient component along the

Y axis, $\partial n / \partial y$, is zero, and the equation for y takes the form

$$\frac{d}{ds} \left(n \frac{dy}{ds} \right) = 0, \quad (54)$$

which immediately implies

$$n \frac{dy}{ds} = \text{const} \quad (55)$$

Refer to the schematic in Fig. 3. Denote the values of n and ε at the point (x_0, y_0) as $n_0 = \sqrt{\varepsilon_0}$, where ε_0 is calculated as in (52). The direction vector component $dy/ds = \sin \alpha$, where α is the angle between the ray direction \mathbf{v}_0 and $-\nabla\varepsilon_0$, which is the X axis here. Therefore, the constant in (55) can be presumed in the form $n_0 \sin \alpha$, so

$$\frac{dy}{ds} = \frac{n_0}{n} \sin \alpha \quad (56)$$

Using the relationship $dx^2/ds^2 + dy^2/ds^2 = 1$ and excluding ds , we arrive at the differential equation

$$\frac{dx}{\sqrt{\varepsilon - \varepsilon_0 \sin^2 \alpha}} = \frac{dy}{\sqrt{\varepsilon_0} \sin \alpha} \quad (57)$$

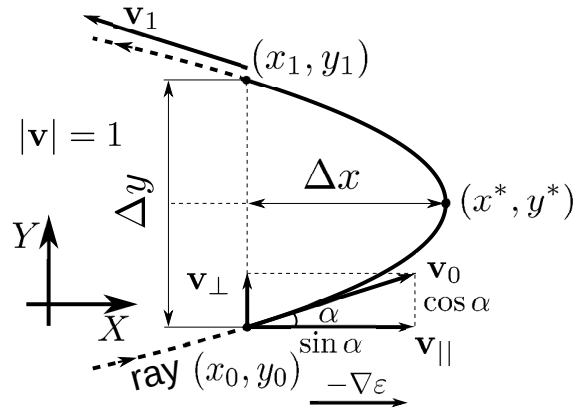


Fig. 3.— Parameters of a ray trajectory approximation by the quadratic parabola in the XY plane. The X axis is aligned with the negated dielectric permittivity gradient, $-\nabla\varepsilon$. The direction cosines' vector \mathbf{v}_0 at the point (x_0, y_0) is decomposed into two components, \mathbf{v}_{\parallel} along the X and \mathbf{v}_{\perp} along the Y , with the lengths equal to $\cos \alpha$ and $\sin \alpha$, respectively. When the ray leaves the parabola at the point (x_1, y_1) , its x coordinate remains the same, but y changes by Δy , equal to the doubled distance from y_0 to the parabola vertex y^* along the Y axis.

Since ε is a linear function (53), $\varepsilon(x) = \varepsilon_0 + (x - x_0)\varepsilon'_0$, where $\varepsilon'_0 = d\varepsilon/dx|_{x=x_0}$, so Eq. (57) can be integrated as

$$\int_{x_0}^x \frac{dx}{\sqrt{\varepsilon'_0 x + \varepsilon'_0 x_0 - \varepsilon_0 \cos^2 \alpha}} = \int_{y_0}^y \frac{dy}{\sqrt{\varepsilon_0} \sin \alpha} \quad (58)$$

to yield the solution in the form $x = x(y)$:

$$x = x_0 - \frac{\varepsilon_0}{\varepsilon'_0} \cos^2 \alpha + \frac{1}{\varepsilon'_0} \left(\sqrt{\varepsilon_0} \cos \alpha + \frac{\varepsilon'_0}{2\sqrt{\varepsilon_0} \sin \alpha} (y - y_0) \right)^2 \quad (59)$$

This second order parabola equation describes the electromagnetic ray trajectory for linearly distributed ε . Its vertex point (x^*, y^*) coordinates are

$$y^* = y_0 - \frac{2\varepsilon_0}{\varepsilon'_0} \cos \alpha \sin \alpha \quad (60a)$$

$$x^* = x_0 - \frac{\varepsilon_0}{\varepsilon'_0} \cos^2 \alpha \quad (60b)$$

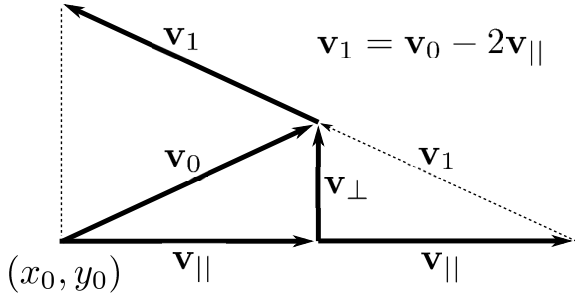


Fig. 4.— The ray direction \mathbf{v}_1 at the opposite branch of the parabola after the parabola switching or Snell's reflection.

We intend to avoid tracing the points lying on the parabola. Assume the ray has already traveled from the point (x_0, y_0) all the way to the axially symmetric point (x_1, y_1) at the opposite branch. In three-dimensional case its position and direction have changed to $(\mathbf{r}_1, \mathbf{v}_1)$. We need to find the increment $\Delta \mathbf{r}$ such that

$$\mathbf{r}_1 = \mathbf{r}_0 + \Delta \mathbf{r} \quad (61)$$

Note that $|\Delta \mathbf{r}| = \Delta y = 2(y^* - y_0)$ and $\varepsilon'_0 = -|\nabla \varepsilon_0|$ because $\varepsilon' < 0$ in the considered vicinity. Using (60a) yields the length of the increment:

$$|\Delta \mathbf{r}| = \frac{4\varepsilon_0}{|\nabla \varepsilon_0|} \cos \alpha \sin \alpha \quad (62)$$

In the chosen XY coordinates $\Delta \mathbf{r}$ points in the Y direction. Decompose \mathbf{v}_0 into its X and Y components $\mathbf{v}_{||}$ and \mathbf{v}_{\perp} ,

$$\mathbf{v}_0 = \mathbf{v}_{||} + \mathbf{v}_{\perp} \quad (63)$$

Here $|\mathbf{v}_0| = 1$, $|\mathbf{v}_{||}| = \cos \alpha$, and $|\mathbf{v}_{\perp}| = \sin \alpha$. We can state that the vector increment $\Delta \mathbf{r}$ should be made in the Y , i.e. \mathbf{v}_{\perp} , direction, so

$$\Delta \mathbf{r} = |\Delta \mathbf{r}| \frac{\mathbf{v}_{\perp}}{|\mathbf{v}_{\perp}|} \quad (64)$$

Since α is the angle between $-\nabla \varepsilon_0$ and \mathbf{v}_0 ,

$$\cos \alpha = |\mathbf{v}_{||}| = \frac{\mathbf{v}_0 \cdot (-\nabla \varepsilon_0)}{|\nabla \varepsilon_0|}, \quad (65)$$

whence the vector increment from \mathbf{r}_0 to \mathbf{r}_1 at the opposite branch of the parabola is

$$\Delta \mathbf{r} = 4\varepsilon \left(-\frac{\mathbf{v}_0 \cdot \nabla \varepsilon_0}{|\nabla \varepsilon_0|^2} \right) \mathbf{v}_{\perp} \quad (66)$$

From (53) the (hypothetical) distance to the critical surface is $L = 1/|\nabla \varepsilon_0|$. With $\cos \alpha$ from (65), we introduce a useful expression

$$L \cos \alpha = -\frac{\mathbf{v}_0 \cdot \nabla \varepsilon_0}{|\nabla \varepsilon_0|^2}, \quad (67)$$

using which the increment (66) can be written as

$$\Delta \mathbf{r} = 4\varepsilon L \cos \alpha \mathbf{v}_{\perp} \quad (68)$$

The new ray direction \mathbf{v}_1 is calculated from the geometrical considerations shown in Fig. 4 as

$$\mathbf{v}_1 = \mathbf{v}_0 - 2\mathbf{v}_{||} \quad (69)$$

To obtain the vector $\mathbf{v}_{||}$, we multiply its absolute value $|\mathbf{v}_{||}|$ from (65) by the unity vector along the X axis, which is $-\nabla \varepsilon_0/|\nabla \varepsilon_0|$, to get the result:

$$\mathbf{v}_{||} = \frac{\mathbf{v}_0 \cdot (-\nabla \varepsilon_0)}{|\nabla \varepsilon_0|^2} \nabla \varepsilon_0, \quad (70)$$

or, using the (67) notation,

$$\mathbf{v}_{||} = -L \cos \alpha \nabla \varepsilon_0, \quad (71)$$

Thus, after the parabola switching, the new ray position and direction are

$$\mathbf{r}_1 = \mathbf{r}_0 + 4\varepsilon L \cos \alpha (\mathbf{v}_0 + L \cos \alpha \nabla \varepsilon_0) \quad (72a)$$

$$\mathbf{v}_1 = \mathbf{v}_0 + 2L \cos \alpha \nabla \varepsilon_0 \quad (72b)$$

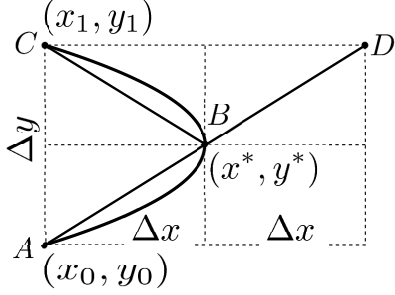


Fig. 5.— The length of parabolic segment ABC is approximated by the added lengths of two parabolic chords AB and BC . This length equals that of the line segment AD .

For the purposes of path integration in line with the trajectory calculation, the integrand is multiplied by the length of every step ds . In case of the parabola switching the integrand is multiplied by the length of the parabola segment, ds_p , from \mathbf{r}_0 to \mathbf{r}_1 . Assuming this length is small enough it can be replaced by the length of two straight line segments connecting the points (in XY coordinates) (x_0, y_0) , the parabola vertex (x^*, y^*) , and (x_1, y_1) , as shown in Fig. 5. Denote as Δx the distance from (x_0, y_0) to (x^*, y^*) along the X axis or, which is the same, along the vector $-\nabla\varepsilon_0$ (see also Fig. 3). Then the parabola length approximation is

$$ds_p = \sqrt{(2\Delta x)^2 + \Delta y^2} \quad (73)$$

We already know that $\Delta y = |\Delta \mathbf{r}|$. From (60b) and using (67) we can find:

$$\Delta x = \varepsilon(L \cos \alpha)^2 |\nabla \varepsilon_0|. \quad (74)$$

6.2.2. Linear reflection

The criterion (51) is based on the linear forward approximation of ε , and sometimes it works incorrectly if the plasma density distribution near the critical surface is highly nonlinear (for example, exponential, as in the chromosphere). Under these conditions the calculated new point of the ray, \mathbf{r}_1 , appears in the region with $\rho > \rho_{cr}$, which is impossible in the physical reality. To fix this condition the algorithm stores in memory the previous ray position and direction $(\mathbf{r}_{-1}, \mathbf{v}_{-1})$.

When the penetration is detected, the algorithm restores the ray state to one step back:

$$(\mathbf{r}_0, \mathbf{v}_0) \leftarrow (\mathbf{r}_{-1}, \mathbf{v}_{-1}). \quad (75)$$

The parabola switching mechanism in this situation can not be relied upon because the linear Taylor series approximations similar to (52) have already failed and the parabola parameters would be calculated incorrectly. The algorithm uses the Newton's method to find the length of step ds along the direction \mathbf{v}_0 such that the next ray point, \mathbf{r}_1 , lies on the critical surface with some small clearance Tol_ε . Then the algorithm performs linear reflection according to the Snell law. Since this conditions only occur at high frequencies when the rays are close to straight lines, this procedure does not deteriorate the algorithm's precision.

The Newton's algorithm is based on stepwise approximation:

$$ds_{i+1} = ds_i - \frac{\varepsilon_i}{\nabla_v \varepsilon_i}, \quad (76)$$

where $\nabla_v \varepsilon_i = \mathbf{v}_0 \cdot \nabla \varepsilon_i$ is the directional derivative of ε_i along the vector \mathbf{v}_0 , so the calculations are performed according to the scheme

$$ds_{i+1} = ds_i - \frac{\varepsilon_i}{\mathbf{v}_0 \cdot \nabla \varepsilon_i}, \quad (77)$$

The process stops when $|\varepsilon_i| \leq Tol_\varepsilon$. The ray direction is then corrected according to the Snell's law. Its geometry is the same as for the parabola switching shown in Fig. 4, so

$$\mathbf{v}_1 = \mathbf{v}_0 - 2\mathbf{v}_{||} \quad (78)$$

where $\mathbf{v}_{||}$ is calculated as in (71), and the next algorithmic step is performed with the last ds value immediately from the critical surface.

7. Testing and validation

The software implementation of the ray tracing algorithm comprises computer programs in the Fortran 90 and C languages. As an example of the algorithm validation, the ray trajectories in a hypothetical medium with the linear dielectric permittivity ε distribution have been obtained numerically using the algorithm and compared with the exact solutions. The results are shown in Fig. 6.

The permittivity ε linearly falls off along the X axis starting from 1 at $x = 0$ down to 0 at some distance L , as given by Eq. (53). The ray trajectories in this medium have been shown to

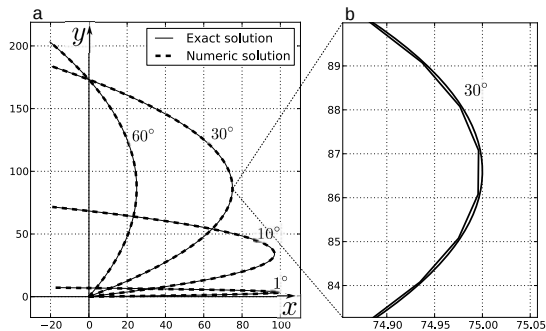


Fig. 6.— Comparison of the numerically simulated ray trajectories for several angles of incidence, 1° , 10° , 30° , and 60° , with the exact ray traces. In panel **a** the simulated ray curves, shown in thick dashed lines, overlap the exact parabolic solutions, plotted in solid thin lines. Panel **b** shows a closer view of short segments of the 30° traces near the reflection point at $x = 75$ calculated by the ray tracing algorithm (segmented line) and the exact solution (79) (smooth, solid line). Notice the scales of the axes.

be parabolas described by Eq. (59). We chose the distance $L = 100$ of conditional units (they might be solar radii, for example), and set the starting point \mathbf{r}_0 at the coordinate origin $(0, 0, 0)$. Here the ray equation (59) takes the form

$$x = L \cos^2 \alpha - L \left(\cos \alpha - \frac{1}{2L \sin \alpha} y \right)^2, \quad (79)$$

where α is the angle of incidence on the critical surface at $x = L$. The results of comparison are presented in panel **a** of Fig. 6. Four angles α were selected: 1° , 10° , 30° , and 60° . The exact solutions calculated by (79) are plotted in thin solid lines; the ray traces created by the algorithm are plotted over them as thicker dashed lines. The dashed curves cover the solid ones, so one can conclude the numerical solutions are essentially precise. In panel **b** of Fig. 6 the differences between the numerical and exact solutions are more discernible because only a short piece of the trajectory in the vicinity of the parabola vertex is shown.

8. Example applications

The algorithm has been applied for solar studies and shown good results. A series of numerical experiments was conducted to simulate the bright-

ness temperature distribution, T_B , across the solar disk as seen from the earth, in the wide frequency range from 10 MHz to 3 GHz. The calculation of T_B requires the ray tracing. We used different electron density distributions, N_e (cm^{-3}), for the corona and the chromosphere. The coronal N_e was approximated by the Saito (1970) model:

$$N_e(r, \theta) = 3.09 \times 10^8 r^{-16} (1 - 0.5 \cos \theta) + 1.56 \times 10^8 r^{-6} (1 - 0.95 \cos \theta) + 0.0251 \times 10^8 r^{-2.5} (1 - \sqrt{\cos \theta}), \quad (80)$$

where r is distance in solar radii, R_\odot , from the sun center and θ is the heliographic colatitude. In the chromosphere, up to 9,000 km from the photosphere, we used the Cillie & Menzel (1935) model:

$$N_e(r) = 5.7 \times 10^{11} e^{-7.7 \times 10^{-4} (R_\odot (r-1) - 500)}, \quad (81)$$

and in the layer between the chromosphere and corona, for the altitudes from 9,000 km to 11,000 km, a smooth polynomial patch function was used.

Electromagnetic Rays Refracting Near Sun at 80.0 MHz

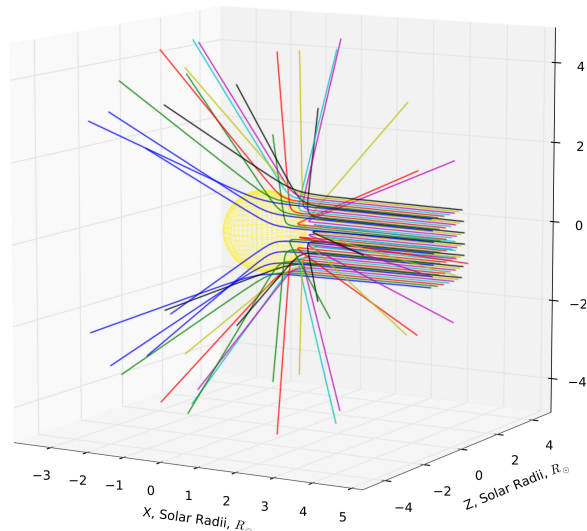


Fig. 7.— The result of numerical simulation of a beam of electromagnetic ray traces at 80 MHz in the solar corona. The square cross-section beam consists of 7×7 evenly spaced rays directed along the X axis in the HEE coordinate system (Fränz & Harper 2002), i.e. from the earth. The sun is shown as a yellow sphere.

In Fig. 7 is shown a bunch of the computed ray trajectories at 80 MHz, refracting in the coronal and chromospheric plasmas. The $7 \times 7 = 49$ evenly

spaced rays comprise a beam converging to a point at the earth distance (here $215 R_{\odot}$), where the rays can be displayed as a 7×7 -pixel raster image. Note that in our experiments with the ray-tracing algorithm the typical raster sizes were from 100×100 to 1000×1000 and more; the beam in Fig. 7 is shown for illustrative purposes only. As seen, the rays arriving at the earth to form an image at 80 MHz can carry information from very different heliospheric regions due to differences in refraction across the image plane.

Fig. 8 shows the results of ray tracing at 200 MHz in the XZ plane of the the HEE (Fränz & Harper 2002) coordinate system (the X points from the sun center at the earth). The rays make up an envelope outlining the critical surface, which is at approximately $1.2R_{\odot}$ from the sun center.

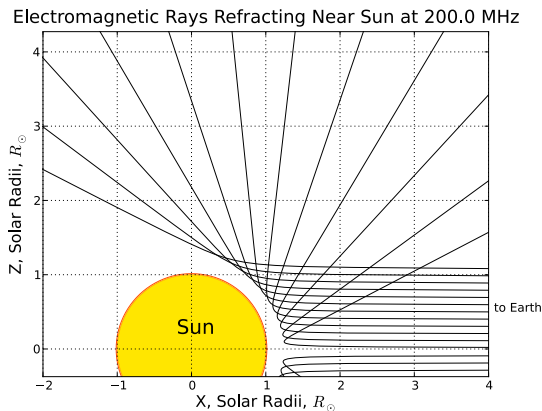


Fig. 8.— Refraction in the corona at 200 MHz in the XZ plane of the HEE coordinate system (Fränz & Harper 2002). The X points at the earth, the Z is normal to the ecliptic plane. The set of propagating rays is shown in thin solid lines. The zone of avoidance close to the solar surface, outlined by the envelope of rays, is clearly visible at $1.2R_{\odot}$.

The higher the frequency, the deeper the electromagnetic rays penetrate into the solar vicinity. Fig. 9 helps estimate the solar distances where the rays at different frequencies start to significantly change the direction. The two thin beams of rays are directed parallel to the $HEE X$ axis at the Z distances of $0.18R_{\odot}$ and $0.67R_{\odot}$, respectively. Each beam includes rays at the frequencies 10, 18, 40, 80, 200 MHz, and 3 GHz. The Fig. 9 can be also viewed as the “spectral decomposition”. One

can notice that at 3 GHz the rays are virtually straight lines.

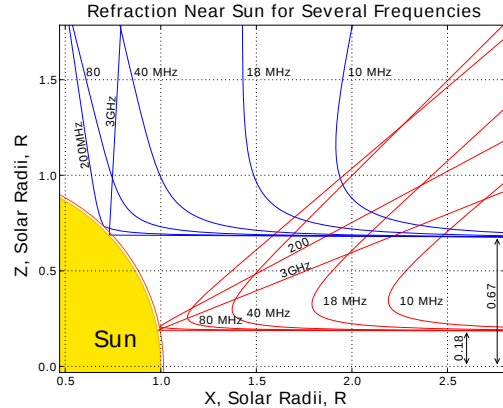


Fig. 9.— Refraction near the sun for several frequencies (“spectral decomposition”). Two thin beams, each composed of the frequencies 10, 18, 40, 80, 200 MHz, and 3 GHz, are directed along the X axis in the XZ plane in the HEE coordinates (Fränz & Harper 2002). The X points at the earth, the Z is normal to the ecliptic plane. The beams’ axes are at $z = 0.18R_{\odot}$ and $z = 0.67R_{\odot}$. One can see the observations at different frequencies are dominated by different layers of the corona.

9. Conclusions

The proposed algorithm is intended for efficient computation of electromagnetic ray traces in the heliospheric plasmas in parallel with integration over the ray paths. To be fast, it is based on a difference scheme of the second order of precision, but it has a property of conserving the direction cosine vector length of the computed trajectory. With this benefit, the algorithm maintains sufficient precision. The difference scheme is only a part of the algorithm: besides, it incorporates several mechanisms for adaptive estimation of the optimal step and prevention of occasional ray penetrations into the regions where the plasma frequencies are higher than the own ray frequency.

The algorithm has been tested on problems of the solar disk image simulation, and it demonstrated good speed, precision, and robustness. We presented here some results pertaining to the ray traces calculation only; the main results will be published in a separate paper. However, we can

conclude that, as seen from Fig. 9, observations at different frequencies are dominated by different layers of the corona and chromosphere. The broad band observations could help reveal the large scale structures in these domains, which can be likened to peeling the layers of an onion bulb. The new high-resolution radiotelescope MWA with its frequency range from 80 to 300 MHz therefore will be an effective instrument in the solar studies. The algorithm and software described in this paper were intended for use as the analysis tool for the MWA solar images.

However we should specially point out that the algorithm applications are in no way confined to the MWA project only. The algorithm can be used for virtually any radioastronomical study because of its very wide frequency range.

Among possible future improvements to the algorithm we could mention the plans on employment of the multi-core, hyperthreading, and multi-channel-memory powers of the modern computers. The problem of simultaneous computation of many ray trajectories can be effectively decomposed into several threads, each running on a separate CPU, because the rays in a beam are calculated independently.

ACKNOWLEDGEMENTS

This work was supported by a NSF grant to the MIT Haystack Observatory. MWA is a large international collaboration, the partner institutions for which are listed below. The US part of the MWA collaboration is funded by the NSF Astronomy and Atmospheric Sciences Divisions.

REFERENCES

- Boris, J., Relativistic Plasma Simulation - Optimization of a Hybrid Code, *Proc. 4th Conf. on the Numer. Simulation of Plasmas*, Office of Naval Research, Arlington, Va., pp. 3-67, 1970
- Cillie, G. G., and Menzel, D. H., *Harv. Coll. Obs. Circ.*, No. **410**, 1935.
- Crank, J. and P. Nicolson, A practical method for numerical evaluation of solutions of partial differential equations of the heat conduction type, *Proc. Camb. Phil. Soc.* **43**: 5067, DOI 10.1007/BF02127704, 1947.
- Fränz, M. and Harper, D., Heliospheric coordinate sys-

tems, *Planetary and Space Science*, Vol. **50**, Issue 2, pp. 217-233, 2002

Haselgrove, J., Ray Theory and a New Method for Ray Tracing, *The Physics of the Ionosphere*, London, Physical Society, pp. 355-364, 1955.

Hockney, R. W. and J. W. Eastwood, Computer simulation using particles, *McGraw-Hill*, 1988

Saito, K., A non-spherical axisymmetric model of the solar K corona of the minimum type, *Ann. Tokyo Astron. Obs.*, Second Ser., vol. **12**, pp. 53-120, 1970

Walker, A.D.M., Ray Tracing in the Magnetosphere, *Radio Science Bulletin*, **327**, pp. 26-38, 2008

This 2-column preprint was prepared with the AAS L^AT_EX macros v5.2.